Evolution of atmospheric age of particles and its implications for the formation of a severe haze event in eastern China

Xiaodong Xie[1], Jianlin Hu[1*], Momei Qin[1], Song Guo[2], Min Hu[2], Dongsheng Ji[3], Hongli Wang[4], Shengrong Lou[4], Cheng Huang[4], Chong Liu[5], Hongliang Zhang[6], Qi Ying[7], Hong Liao[1], Yuanhang Zhang[2]

5

[1] Jiangsu Key Laboratory of Atmospheric Environment Monitoring and Pollution Control, Collaborative Innovation Center of Atmospheric Environment and Equipment Technology, Nanjing University of Information Science & Technology, Nanjing 210044, China
[2] State Key Joint Laboratory of Environmental Simulation and Pollution Control, College of
10 Environmental Sciences and Engineering, Peking University, Beijing, 100871, China
[3] State Key Laboratory of Atmospheric Boundary Layer Physics and Atmospheric Chemistry, Institute of Atmospheric Physics, Chinese Academy of Sciences, Beijing, 100191, China
[4] State Environmental Protection Key Laboratory of Formation and Prevention of Urban Air Pollution Complex, Shanghai Academy of Environmental Sciences, Shanghai, 200233, China
15 [5] CMA Earth System Modeling and Prediction Centre, State Key Laboratory of Severe Weather, China Meteorological Administration (CMA), Beijing 100081, China
[6] Department of Environmental Science and Engineering, Fudan University, Shanghai 200438, China
[7] Zachry Department of Civil Engineering, Texas A&M University, College Station, Texas 77843, USA

20 *Corresponding author: Jianlin Hu (jianlinhu@nuist.edu.cn)

Abstract

Atmospheric age reflects how long particles have been suspended in the atmosphere, which is closely associated with the evolution of air pollutants. Severe regional haze events occur frequently in China, influencing air quality, human health, and regional climate. Previous

25   studies have explored the characteristics of mass concentrations and compositions of fine particulate matter ($PM_{2.5}$) during haze events, but the evolution of atmospheric age remains unclear. In this study, the age-resolved UCD/CIT model was developed and applied to simulate the concentration and age distribution of $PM_{2.5}$ during a severe regional haze episode in eastern China. The results indicated that $PM_{2.5}$ concentrations in the North China Plain (NCP)

30   gradually accumulated due to stagnant weather conditions at the beginning stage of the haze event. Accordingly, the atmospheric age of elemental carbon (EC), primary organic aerosol (POA), sulfate (SO_4^{2-}), and secondary organic aerosol (SOA) gradually increased. The subsequent $PM_{2.5}$ concentration growth was driven by the local chemical formation of nitrate (NO_3^-) under high relative humidity. The newly formed NO_3^- particles led to a decrease in the

35   mean atmospheric age of the NO_3^- particles. During the regional transport stage, aged particles from the NCP moved to the downwind Yangtze River Delta (YRD) region, leading to a sharp increase in $PM_{2.5}$ concentrations and the average age of EC, POA, SO_4^{2-}, and SOA. In contrast, the average age of NO_3^- and ammonium remained unchanged or even slightly decreased due to continuous local formation in the YRD region. Different evolution of the atmospheric age

40   among these components provides a unique perspective on the formation of $PM_{2.5}$ components during the regional haze event. The information can also be used for designing effective control strategies for different components of $PM_{2.5}$.

Keywords: Atmospheric age; Haze event; Regional transport; Chemical transport model; Eastern China

45 **1. Introduction**

Haze pollution is a chronic environmental issue in China, influencing atmospheric visibility (Li et al., 2019; Pui et al., 2014), human health (Wang et al., 2021a; Lelieveld et al., 2015; Cohen et al., 2017), ecosystem (Xie et al., 2020; Gu et al., 2002; Cirino et al., 2014), and climate (Ramanathan et al., 2001; Seinfeld et al., 2016; IPCC, 2021). Fine particulate matter, also

50 known as $PM_{2.5}$, the major pollutant during haze days, is either directly emitted into the atmosphere or formed from precursor gases through chemical processes. Although the annual mean $PM_{2.5}$ concentrations in Chinese megacities have been substantially reduced in recent years because of the strict emission control measures (Wang et al., 2019; Zhang et al., 2019b), severe regional haze pollution ($PM_{2.5} > 150\ \mu g\ m^{-3}$) still frequently occurs in densely populated

55 regions, such as the North China Plain (NCP) and the Yangtze River delta (YRD) (An et al., 2019).

Intensive pollutant emissions and unfavorable meteorology are two key factors controlling haze formation. NCP and YRD are two major city clusters in eastern China with intensive anthropogenic emissions. Previous studies have revealed that severe winter haze events in the

60 NCP were initialized by the accumulation of local emissions under stable weather conditions and further deteriorated by rapid secondary formation (An et al., 2019; Zheng et al., 2015b). Polluted air masses in the NCP are rapidly eliminated by the strong prevailing northwesterly wind and moved to downwind YRD regions (Wang et al., 2021c). During the long-range transport, freshly emitted particles gradually age and mix with secondary inorganic and organic

65 species, further influencing regional climate and air quality through aerosol-planetary boundary layer (PBL) interaction (Huang et al., 2020; Zhang et al., 2021).

The atmospheric age of an air pollutant, defined as the time since it is emitted or formed, provides a unique perspective on the evolution of pollutants in the atmosphere (Wagstrom and Pandis, 2009; Ying et al., 2021; Zhang et al., 2019a). Unlike the lifetime or residence time of

70 pollutants, atmospheric age refers to the time that a single particle remains in the atmosphere at a given location and time, which can better reflect its instantaneous physical and chemical

properties (Chen et al., 2017c). However, measuring and calculating the atmospheric age of air pollutants is difficult because of their chemical nonlinearity and process complexity. Previous studies have attempted to track particle age distributions by adding tracers in Lagrangian

75   trajectory models such as FLEXPART (Stohl et al., 2003). However, due to simplified chemistry, this method cannot accurately determine the age distributions of secondary species. Some other studies estimated the photochemical age of an air mass using the ratio of hydrocarbons, including toluene/benzene and ethylbenzene/benzene (Chu et al., 2021; Parrish et al., 2007). Since the oxidation rates of these hydrocarbons by hydroxyl (OH) radicals span

80   several orders of magnitude, the hydrocarbon ratios change with photochemical aging (Chen et al., 2021). By this definition, the photochemical age determines the degree of photochemical processing associated with OH radicals rather than the physical age of pollutants (Irei et al., 2016).

A few attempts were made to track the age distribution of aerosols using chemical transport

85   models (CTMs) (Han and Zender, 2010; Wagstrom and Pandis, 2009; Wu et al., 2017). CTMs can reproduce the evolution of pollutants in the atmosphere (including emission, transport, deposition, and chemical transformation). Zhang et al. (2019a) introduced a dynamic age-bin updating algorithm in the source-oriented University of California, Davis/California Institute of Technology (UCD/CIT) air quality model to track the age distribution of primary $PM_{2.5}$. In

90   their study, chemical variables in UCD/CIT model were expanded with one more dimension to represent pollutants with different atmospheric ages. More recently, this dynamic age-bin updating algorithm was expanded to include gaseous precursors to determine the age distribution of all primary and secondary inorganic compounds in the Community Multiscale Air Quality (CMAQ) model (Ying et al., 2021). In this study, we further developed an age-

95   resolved UCD/CIT model to track the atmospheric age distribution of various primary and secondary components of $PM_{2.5}$ based on the method used in the CMAQ model. Then we applied the model to investigate the evolution of the concentrations and ages of the major $PM_{2.5}$ components during a typical winter haze episode in eastern China.

2. Methods

100 **2.1 Description of UCD/CIT Model**

The source-oriented UCD/CIT air quality model (Held et al., 2004; Hu et al., 2014; Hu et al., 2015; Kleeman and Cass, 2001; Ying et al., 2007; Ying and Kleeman, 2006) was used in this study to simulate air quality in eastern China. The UCD/CIT model is a 3-dimensional Eulerian regional CTM with detailed chemistry and aerosol mechanisms. Details about the fundamental

105 algorithms used in UCD/CIT model can be found in the above references. Briefly, gas-phase chemistry is modeled by the SAPRC-11 chemical mechanism (Carter and Heo, 2013). Aerosols are represented using a sectional approach with 15 log-spaced size bins encompassing 10 nm– 10 μm. Thermodynamic equilibrium for inorganic aerosols is calculated by ISORROPIA (Nenes et al., 1998). Secondary organic aerosol (SOA) treatment is based on the two-product

110 model used in the Community Multiscale Air Quality (CMAQ) model, including a total of 19 semi-volatile or nonvolatile species from seven precursors (Carlton et al., 2010).

In most existing air quality models, particles from diverse emission sources are mixed. However, the UCD/CIT model applies a source-oriented framework in which primary and secondary particles from each source category are tracked separately through the calculation

115 of all major atmospheric processes, such as advection, diffusion, deposition, and gas-particle partitioning. Thus, the source contributions to regional particle concentrations can be evaluated. Zhang et al. (2019a) expanded the source-oriented UCD/CIT model to track the age distribution of elemental carbon (EC) in the atmosphere. In this study, we implemented the atmospheric age distribution modeling framework (Ying et al., 2021) to track the age distribution of both

120 primary and secondary aerosols. The age distribution of SOA was added to the framework, making it possible to have complete age-resolved modeling of secondary aerosols.

The age-resolved UCT/CIT model employs a sectional approach to track particles of different atmospheric ages (n age bins). Freshly emitted or formed particles at each model time step are set to the lowest age bin. At a fixed age-bin updating frequency ($\Delta\tau$), particles in the lower

125 age bin would be moved to the higher age bin successively. Particles in the last age bin represent

those older than the highest explicit age. The average age of particles in the ith age bin ($\overline{\tau_i}$) is

approximately equal to the middle of that period:

$$\overline{\tau_i} = (i - \frac{1}{2})\Delta\tau, \quad i = 1, 2, ..., n \tag{1}$$

The average age of particles can be calculated by

130
$$\overline{\tau} = \sum \frac{\tau_i C_i}{\sum C_i} \tag{2}$$

2.2 Model setup

The age-resolved UCD/CIT model was run from 21 December 2017 to 2 January 2018, with

the first 4 days as the spin-up period to minimize the impact of initial conditions. The model

domain has a horizontal resolution of 36 km encompassing eastern China and a vertical

135 structure of 16 layers with 10 layers below 1 km. Hourly meteorological inputs were generated

by the Weather Research Forecasting (WRF) model version 4.2 with initial and boundary

conditions from the 1.0° × 1.0° National Centers for Environmental Prediction Final (NCEP

FNL) operational global analyses dataset. More details on the WRF model configuration can

be found in Xie et al. (2022a).

140 Anthropogenic emissions were taken from MEIC (the Multi-resolution Emission Inventory for

China) v1.3 with a spatial resolution of 0.25° ×0.25° (Zheng et al., 2018). FINN (Fire

INventory from NCAR) v1.5 with 1 km resolution (Wiedinmyer et al., 2011) and MEGAN

(Model of Emissions of Gases and Aerosols from Nature) (Guenther et al., 2006) driven by

meteorological inputs from WRF were used to provide wildfire and biogenic emissions,

145 respectively. Total particle-phase emissions from the above mentioned sources were

transformed into size-resolved emissions based on measured source profiles (Kleeman et al.,

2008; Robert et al., 2007a; Robert et al., 2007b). In addition, sea salt and dust emissions were

calculated online within the model based on wind speed and land use type, as described in Hu

et al. (2015).

150   A total of 9 age bins were configured to determine the age distribution of particles in this study.
        The age-bin updating frequency was set to 12 h in our base simulation so that we could
        explicitly track particle ages up to 96 h. However, $PM_{2.5}$ concentrations can grow explosively
        during our study period within several hours. Thus, another four simulations with age-bin
        updating intervals of 1, 3, 6, and 8 h were also conducted to better reflect the age distribution

155   of particles. Results from different simulations were combined by replacing the low time
        resolution simulations with the corresponding high time resolution results (Ying et al., 2021).
        The simulated concentrations of $PM_{2.5}$ and its major components from the age-resolved model
        show good agreement with the original UCD/CIT model (Figure S1), confirming that the
        dynamic age-bin updating algorithm will not change the concentration prediction. The

160   computational burden of the age-resolved UCD/CIT model with 9 age bins is ~3 times slower
        than the original model.

2.3 Field observations

        Hourly meteorological data, including 2-m air temperature (T2), 10-m wind speed (WS) and
        direction (WD), and 2-m relative humidity (RH) were collected from 171 routine weather

165   stations in eastern China (**Figure 1**) from the Chinese National Meteorological Center
        (http://data.cma.cn/en). Surface $PM_{2.5}$ observations were acquired from the national air quality
        monitoring network developed by the China National Environmental Monitoring Center
        (http://www.cnemc.cn/en). Measurements on aerosol composition were conducted at four main
        cities in eastern China, including Beijing, Jinan, Nanjing, and Shanghai. Water-soluble

170   inorganic ions (WSIIs, including nitrate (NO_3^-), sulfate (SO_4^{2-}), and ammonium (NH_4^+)) were
        measured by an online analyzer (MARGA, model ADI 2080, Applikon Analytical B. V. Corp.,
        Netherlands) with a $PM_{2.5}$ cyclone inlet in Jinan, Nanjing, and Shanghai (Shu et al., 2019). In
        Beijing, the mass concentrations of WSIIs were analyzed by two ion chromatography systems
        (DIONEX ICS2000 and ICS2500 for cations and anions, respectively) (Tan et al., 2018).

175   Carbonaceous components (organic carbon (OC) and EC) in four cities were analyzed with a
        carbon analyzer (model RT-4, Sunset Laboratory Inc., USA) based on the thermal-optical

transmittance method (Wang et al., 2016b). More details about the principles and operation of the above instruments can be found in the corresponding references.

The incremental mass ratio (IMR) proposed by Tan et al. (2018) was adopted in this study to

180   determine the aerosol components that drive the particle concentration growth during the haze episode. Briefly, the IMR of a certain component i (IMR_i) is calculated as the ratio of the increment of component i (ΔC_i) to the increment of PM$_{2.5}$ ($\Delta PM_{2.5}$) total mass during the PM$_{2.5}$ growth process:

$$IMR_i = \frac{\Delta C_i}{\Delta PM_{2.5}} \times 100 \qquad (3)$$

185   Thus, the contribution of each chemical composition to the PM$_{2.5}$ increment can be calculated.

3. Results

3.1. Episode description and model evaluation

Figure 2 shows a severe regional haze episode over eastern China spanning from 25 December 2017 to 2 January 2018. The time series of PM$_{2.5}$ concentrations in eastern China indicates that

190   PM$_{2.5}$ gradually accumulated in the NCP from 25–28 December 2017 under the condition of low wind speed (~2 m s^{-1}) and increasing RH (**Figure S1**), which is identified as the accumulation stage. Severe haze pollution characterized by high PM$_{2.5}$ concentrations (> 150 μg m^{-3}) persisted from the night of 28 December to the morning of 30 December, while the peak value of PM$_{2.5}$ reached 191 μg m^{-3} at 10:00 LT 29 December (stabilization stage). On 30

195   December, a cold front formed in the NCP, where the cold air in front of the Siberian High encountered the warm air from the south (**Figure S2**). As a result, the wind speed increased sharply from 2.5 m s^{-1} to 5.7 m s^{-1} within 6 h, followed by a steep drop in air temperature from 4.3 °C to −7.0 °C (**Figure S1**). Under the influence of strong northwesterly winds, a continuous movement of PM$_{2.5}$ from north to south (i.e., Taiyuan, Linfen, Shijiazhuang, Zhengzhou,

200   Nanjing, and Shanghai) occurred, and the polluted air masses dissipated quickly in the NCP within several hours (dilution stage) (**Figure S3**). Consequently, severe haze pollution formed

Atmospheric
Chemistry
and Physics
Discussions

Open Access

EGU

rapidly in the YRD during 30–31 December due to regional transport from the NCP, with the peak value of $PM_{2.5}$ concentrations greater than 200 µg m^{-3}.

To better explore the characteristics of $PM_{2.5}$ pollution in the YRD, the haze episode was divided into three stages (before, during, and after regional transport) in this study according to $PM_{2.5}$ concentrations and winds (**Figure 2a and 2b**). Before regional transport, $PM_{2.5}$ concentrations in the NCP (> 250 µg m^{-3}) were much higher than those in the YRD (~70 µg m^{-3}). Low wind speed (~2 m s^{-1}) favored the accumulation of air pollutants in the NCP. Meanwhile, southeasterly winds prevailed in the coastal areas of the YRD, bringing less polluted air masses. In the following 1–2 days, eastern China was under the control of strong northwesterly winds (4–5 m s^{-1}) due to the cold front, and the heavily polluted air masses gradually moved from north to south (**Figure 2d**). After the cold front passes, high pressure controls the YRD, leading to subsidence and trapping $PM_{2.5}$ in the PBL. Thus, high concentrations of $PM_{2.5}$ occurred in the YRD with low wind speed, especially in Jiangsu and Shanghai (**Figure 2e**).

The UCD/CIT model well reproduces the observed temporal variations of hourly $PM_{2.5}$ concentrations averaged over the NCP and the YRD during this haze episode with a high correlation coefficient (R > 0.85) and a low bias (NMB < 15%) (**Figure 2b**). High $PM_{2.5}$ concentrations (> 150 µg m^{-3}) with low wind speed over southern Hebei, Shandong, Henan, northern Jiangsu, and Anhui provinces are well captured by the model (**Figure S4**). The simulated $PM_{2.5}$ compositions (SO_4^{2-}, NO_3^-, NH_4^+, EC, and organic matter (OM)) also agree well with the daily-averaged measurements in Beijing, Jinan, Nanjing, and Shanghai (**Figure S5**), with model performance statistics comparable to those in other studies(Shi et al., 2017; Hu et al., 2016; Zhang et al., 2019b). Detailed model evaluation can be found in the Supporting Information.

3.2. Evolution of particle chemical compositions

Figure 3 shows the observed chemical composition evolution in Beijing, Jinan, Nanjing, and Shanghai. SNA increased rapidly and became the major component of $PM_{2.5}$ during the $PM_{2.5}$

Atmospheric
Chemistry
and Physics
Discussions

growth process in all four cities, while the mass fraction of EC and OM in $PM_{2.5}$ decreased. In

230 Beijing and Jinan, located in the NCP, the daily averaged SNA concentrations increased from

10 and 22 $\mu g\ m^{-3}$ on 25 December to 110 and 157 $\mu g\ m^{-3}$ on 29 December, and their mass

fraction in $PM_{2.5}$ increased from ~40% to ~75%. During 25–29 December, the NCP region was

under the control of a uniform pressure field with low horizontal winds (**Figure S2**), and

pollutants gradually accumulated under such stagnant conditions. The observed RH gradually

235 increased, and the maximum exceeded 80% on 28–29 December, which facilitated the

chemical formation of secondary aerosols and accelerated the hygroscopic growth of particles

(Cheng et al., 2016; Sun et al., 2014; Yang et al., 2015). Process analysis also indicates that

chemical formation is the driving process for the growth of SNA in the NCP, with its net

production rate ~3 times larger than that of vertical mixing and horizontal advection during the

240 accumulation stage (**Figure 4a, b**). For YRD cities, Nanjing and Shanghai, daily SNA

concentrations increased sharply by 3–6 times within two days (30–31 December) and

accounted for 78% of the peak $PM_{2.5}$. Horizontal advection played a dominant role during the

explosive growth of air pollutants, with a maximum production rate of 8.1 and 2.7 $\mu g\ m^{-3}\ h^{-1}$

for NO_3^- and SO_4^{2-} respectively (**Figure 4c, d**). The chemical process also contributed

245 obviously to NO_3^- and SO_4^{2-} in Nanjing during the regional transport, indicating the continuous

local formation in the YRD.

NO_3^- exhibited the highest levels among SNA in all four cities. The peak value of NO_3^- was

49, 57, 80, and 51 $\mu g\ m^{-3}$ for Beijing, Jinan, Nanjing, and Shanghai, respectively, contributing

to 25–41% of $PM_{2.5}$ mass concentrations. The IMR of NO_3^- (29–33%) was much higher than

250 that of other components in Beijing, Nanjing, and Shanghai (**Figure 3e**), indicating that NO_3^-

was the driving component during the $PM_{2.5}$ growth process. In Jinan, the IMR of SO_4^{2-} (26%)

was slightly higher than that of NO_3^- (24%). Nevertheless, the mass fraction of NO_3^- in $PM_{2.5}$

during the $PM_{2.5}$ growth process (25–29 December) was 26%, significantly larger than that of

SO_4^{2-} (16%) and NH_4^+ (15%). The higher fraction of NO_3^- in $PM_{2.5}$ and its dominant

255 contribution to the $PM_{2.5}$ growth process have also been pointed out by recent observation and

modeling studies conducted in eastern China during winter haze periods (Shao et al., 2018; Xu

et al., 2019; Xie et al., 2022b).

3.3. Evolution of particle age distribution

The age distribution evolutions of the major $PM_{2.5}$ compositions (EC, SO_4^{2-}, NO_3^-, NH_4^+, POA,

260   and SOA) in Beijing and Shanghai are illustrated in **Figures 5 and 6**. High concentrations of

EC, POA, and SO_4^{2-} typically occurred at low atmospheric ages, with obvious diurnal

variations in both cities. The bimodal distribution of fresh particles was mainly related to the

variations in local emissions and the evolution of PBL. Because the shallow PBL at night was

not conducive to the diffusion of air pollutants, particles emitted during evening rush hours

265   remained in the atmosphere longer than those emitted in the morning. Several hours after being

released, the concentrations of particles dropped rapidly due to the atmospheric dilution process

such as advection and deposition. Nevertheless, under stable weather conditions with low wind

speeds, the dilution effect was weak, and EC, POA, and SO_4^{2-} particles could accumulate in

the atmosphere for a longer time. This can be seen in Beijing from 25–29 December with a

270   gradually increasing mean atmospheric age of EC, POA, and SO_4^{2-}. During this time, relatively

high concentrations of aged EC, POA, and SO_4^{2-} particles (with atmospheric age > 24 h)

together with large contributions from fresh particles (with atmospheric age < 24 h) can also

be observed (e.g., 12:00 to 16:00 LT 28 December). On 30 December, aged EC, POA, and

SO_4^{2-} particles in Beijing were removed sharply by strong northwesterly wind, leading to a

275   steep decrease (from ~40 h to less than 6 h) in their mean atmospheric age. Subsequently, in

Shanghai, the concentration of aged particles increased rapidly during the period from 14:00

LT on 30 December to 02:00 LT on 31 December, indicating the influence of regional transport.

As a result, the mean atmospheric age of EC, POA, and SO_4^{2-} increased from 3–6 h to 47–52

h.

280   Similar to that of EC, POA, and SO_4^{2-}, the average age of SOA gradually increased during the

accumulation stage in the NCP region, and then decreased sharply on 30 December due to the

sweeping effect of the strong northwesterly wind. In YRD, the average age of SOA before the

regional transport was larger than that of EC and POA, although its concentrations were

relatively low. During the regional transport, the average age of SOA increased from ~20 h to ~60 h within several hours. Oligomers of anthropogenic SOA (AOLGA), xylene, toluene, long-chain alkanes, and monoterpenes were found to be the most important precursors, contributing over 95% of the total SOA in Beijing, Jinan, Nanjing, and Shanghai (**Figure S7 and S8**). The contribution of AOLGA increased with atmospheric age in all four cities, while the contributions of xylene, toluene, and long-chain alkanes decreased with age. In the NCP cities, the contribution of AOLGA to total SOA concentrations increased from 35% in the accumulation stage to 48% in the stabilization stage. This is because semi-volatile SOA would not immediately form AOLGA after being released into the atmosphere, and the oligomerization reactions take time.

NO_3^- and NH_4^+ exhibited different age distributions compared to EC, POA, SO_4^{2-}, and SOA. The mean atmospheric age of NO_3^- and NH_4^+ did not show an increasing trend and even decreased on some occasions during the accumulation stage in Beijing and Jinan (**Figures S9 and S10**). Such a low atmospheric age was mainly due to the continuous formation of secondary NH_4NO_3 particles locally (**Figure S11**), which increased the concentrations of fresh particles and decreased the mean age of NO_3^- and NH_4^+. High concentrations of fresh NO_3^- combined with a moderate contribution of aged NO_3^- can also be seen during the explosive growth stage (e.g., 16:00 to 23:00 LT 30 December 2017) in Nanjing and Shanghai, indicating that the continuous local formation with additional help from regional transport together contribute to the high concentrations of NO_3^-. The average atmospheric age of NO_3^- in Jinan, Nanjing, and Shanghai decrease significantly with RH and low average ages are often observed with a high concentration of NO_3^- (**Figure S12**). This confirms our speculation that the rapid chemical formation of NO_3^- under high RH conditions (**Figure S1**) leads to a high concentration of fresh NO_3^- and decreases the mean age of NO_3^-.

The vertical cross sections of the concentrations and mean ages for EC and NO_3^- along the transport route from Beijing to Shanghai (white solid line in **Figure 1**) are shown in **Figures 7 and 8**, while those for SO_4^{2-} and SOA are illustrated in **Figures S13 and S14**. Before the regional transport (e.g., 16:00 LT 28 December 2017), aged particles mainly accumulated in

Atmospheric
Chemistry
and Physics
Discussions
EGU
Open Access

the NCP under slow wind speed (~2 m s^{-1}). The average age of EC, SO$_4^{2-}$, NO$_3^-$, and SOA was approximately 30–50 h, 50–60 h, 20–45 h, and 50–60 h respectively, larger than that in the YRD (15–30 h for EC, 30–50 h for SO$_4^{2-}$, 8–24 h for NO$_3^-$, and 35–45 h for SOA). An obvious vertical gradient of particle age occurred in the YRD, with lower age near the surface and higher age aloft. Due to the accumulation of aged pollutants in the atmosphere under stable weather conditions, the vertical distribution of particle ages was more uniform in the NCP. When the cold front passed through, polluted air masses carrying aged particles gradually moved from the NCP to the YRD under strong northwest wind (>5 m s^{-1}). During this period, high PM$_{2.5}$ concentrations occurred in eastern China and vertically extended up to 1.2 km, forced by the upward motion along the cold front. For EC, SO$_4^{2-}$, and SOA, the average age in the YRD increased significantly within the whole PBL due to the regional transport from the NCP. The maximum age reached 48, 60, and 65 h for EC, SO$_4^{2-}$, and SOA, respectively. For NO$_3^-$, the highest concentration reached 180 μg m^{-3} for regions between Jinan and Nanjing at 08:00 LT on 30 December 2017, which was 2 times the peak value in the NCP before the regional transport (~90 μg m^{-3}). Moreover, the average age of NO$_3^-$ was relatively low (6–24 h) for high-concentration NO$_3^-$ particles, indicating the significant contribution from the local chemical formation.

The age distribution of the major PM$_{2.5}$ chemical compositions (EC, SO$_4^{2-}$, NO$_3^-$, NH$_4^+$, and SOA) in Beijing, Jinan, Nanjing, and Shanghai is shown in **Figure 9**. SO$_4^{2-}$ and SOA exhibited larger atmospheric age than the other three species, with a maximum average age of 84 and 81 h, respectively. In the NCP cities, Beijing and Jinan, more aged particles occurred in the stabilization stage. The average age in Beijing was 45, 76, 55, 61, and 71 h for EC, SO$_4^{2-}$, NO$_3^-$, NH$_4^+$, and SOA respectively, higher than that in the accumulation and dilution stages. It is worth noting that a large fraction (50–60%) of fresh NO$_3^-$ and NH$_4^+$ particles with an age of less than 12 h occurred in Jinan during the stabilization stage, indicating a rapid local formation. In the YRD cities, Nanjing and Shanghai, the mass fraction of aged EC, SO$_4^{2-}$, and SOA particles increased significantly during the regional transport, their average ages were even larger than that in the NCP. This is mainly because of the strong northwesterly wind that

340   brought abundant aged particles from the NCP. NO_3^- and NH_4^+ showed smaller atmospheric

age than SO_4^{2-} and SOA, with an average age of 20–30 h during the regional transport. Fresh

NO_3^- and NH_4^+ particles with atmospheric age of less than 24 h account for more than 70% of

the total mass.

Figures 10 and S15 show the size distribution of the major $PM_{2.5}$ chemical compositions in

345   Beijing and Shanghai. Both EC and POA exhibited bimodal distributions, with a fine-mode

peak at 0.2–0.4 μm and a coarse-mode peak at 1–4 μm, respectively. SOA, SO_4^{2-}, NO_3^-, and

NH_4^+ were mainly concentrated in the fine mode, with a peak at 3–4 μm. The size distribution

of particles with different atmospheric ages was quite different. Aged particles were mainly

concentrated in a larger size range, especially for SOA, SO_4^{2-}, and NO_3^-. For example, SO_4^{2-}

350   with a diameter >0.4 μm in both Beijing and Shanghai showed an atmospheric age of >96 h.

When the accumulation stage evolved into the stabilization stage, the size of SOA, SO_4^{2-}, and

NO_3^- slightly increased in Beijing, while that of EC and POA remained almost unchanged. In

Shanghai, NO_3^- and NH_4^+ were mainly concentrated in the size range of 0.1–0.3 μm before the

regional transport. Their dominant size increased to 0.3–0.7 μm during the regional transport.

355   **4. Discussion**

Our results indicate that the atmospheric age of EC, POA, SO_4^{2-} and SOA increased gradually

during the accumulation stage in the NCP due to air stagnation. The regional transport from the

NCP to the YRD brought in high concentrations of aged primary particles, such as EC and

POA. As a result, the simulated average atmospheric age of EC was ~40 h during the regional

360   transport, which was much higher than the 'experimental' aging time scale to achieve complete

morphology modification and absorption enhancement of BC in Beijing (4.6 h) and Houston

(18 h) (Peng et al., 2016). It could be speculated that the aged EC or POA particles are coated

continuously by the newly formed fresh SNA particles along the transport route, which could

further enhance the light absorption of particles (Bond et al., 2013). Using transmission

365   electron microscopy (TEM), Zhang et al. (2021) observed abundant spherical primary OM

particles coated with secondary aerosols in the YRD during the regional transport, which is

consistent with our findings. Previous studies have confirmed the crucial role of aerosol-PBL

interaction in altering the vertical structure of PBL and the formation and accumulation of haze in eastern China (Huang et al., 2020; Li et al., 2017). Thus, the potential absorption

370 enhancement of aged black or brown carbon particles during the regional transport could amplify the aerosol-PBL interactions and further exacerbate air pollution.

Another interesting finding is that the atmospheric age of NO_3^- remained unchanged or even slightly decreased during the regional transport from NCP to YRD, contrary to the age evolution of SO_4^{2-}. This indicates that SO_4^{2-} is mainly formed upwind and then transported to

375 YRD, while there is a large fraction of NO_3^- is formed locally in YRD. SO_4^{2-} concentrations have been dramatically reduced during the last decade due to desulfurization devices vigorously promoted in coal-fired facilities, and NO_3^- has become the dominant inorganic component of $PM_{2.5}$ in most regions of Eastern China (Sun et al., 2022). Our previous study for January 2013 suggested that NO_x emissions from local sources and adjacent Jiangsu

380 province contributed to nearly 30% of NO_3^- in Shanghai, respectively (Xie et al., 2021). Therefore, NO_3^- reduction can be achieved by cooperative emission controls within the YRD region. Surely, emission reduction actions should be taken a few days in advance to mitigate severe haze pollution under unfavorable weather conditions.

This study is subject to a few limitations. The UCD/CIT model includes SO_4^{2-} formation

385 mechanisms through the gas phase oxidation of SO_2 by OH radicals and the in-cloud aqueous oxidation. However, recent field observations indicated a large contribution from other pathways during winter haze events in China, such as manganese-catalyzed oxidation on aerosol surfaces (Wang et al., 2021b), and aqueous oxidation of SO_2 by NO_2 (Cheng et al., 2016; Wang et al., 2016a). The missing mechanism in the current model leads to a substantial

390 underestimation of SO_4^{2-} (42.3%), which will further affect the age distribution of SO_4^{2-} particles. Since SOA is universally underestimated in current CTMs (Hu et al., 2017), uncertainties may also occur with SOA. Additionally, the discretization of atmospheric age in our model can lead to some uncertainties, especially for the calculation of average atmospheric age (Xie et al., 2022a). Thus, in this study, we run five different simulations with $\Delta\tau$ of 1, 3, 6,

395   8, and 12 h respectively, and combined the results to minimize the effect of discrete age representation.

5. Conclusions

In this study, the age-resolved UCD/CIT model was used to investigate the age distribution of $PM_{2.5}$ during a severe regional haze episode in eastern China in December 2017. Comparison

400   with surface observation shows that the model reasonably captured the spatiotemporal variations of $PM_{2.5}$ and its major chemical compositions. Our results indicate that at the beginning stage of the haze event (25–29 December 2017), the stagnant weather conditions characterized by weak surface wind and high RH facilitated the accumulation and secondary formation of air pollutants, leading to increased $PM_{2.5}$ concentrations in the NCP region. NO_3^-

405   was found to be the dominant chemical composition during this haze episode, contributing to ~30% of $PM_{2.5}$ concentration growth in Beijing, Jinan, Nanjing, and Shanghai. Both the concentration and atmospheric age of EC, POA, SO_4^{2-} and SOA increased gradually during the accumulation stage in the NCP due to weakened atmospheric diffusion capacity, while the atmospheric age of NO_3^- and NH_4^+ remained unchanged because of continuous local formation.

410   During the regional transport stage (30 December), a cold front moved from north to south, bringing aged particles from the NCP to the YRD region and increasing $PM_{2.5}$ concentrations rapidly within hours. Accordingly, the average atmospheric age of EC, POA, SO_4^{2-} and SOA particles in the YRD increased from 5–20 h to 50–60 h. In contrast, continuous local chemical formation resulted in an unexpected decrease in the atmospheric age of NO_3^- and NH_4^+ in the

415   YRD, although the concentrations of aged particles with old atmospheric age increased due to regional transport. The age information provided in this study enhances our understanding of the formation mechanism of haze events and helps design cost-effective control strategies for different $PM_{2.5}$ components.

Code and data availability

420   Hourly $PM_{2.5}$ data used in this study is freely available through the website of http://106.37.208.233:20035/ (last accessed on January 6, 2023). Meteorological observations

used in this study are available from http://data.cma.cn/en (last accessed on January 6, 2023).

The UCD/CIT model outputs are currently available upon request.

Author contributions

425 XX and JH designed research. XX, JH, MQ, HZ and QY contributed to model development, simulations, and data processing. SG, MH, DJ, HW, SL, CH, CL provided the observation data. HL and YZ contributed to result discussion. XX prepared the manuscript and all coauthors helped improve the manuscript.

Competing interests

430 The authors declare that they have no conflict of interest.

Acknowledgments

435 **References**

An, Z., Huang, R., Zhang, R., Tie, X., Li, G., Cao, J., Zhou, W., Shi, Z., Han, Y., Gu, Z., and Ji, Y.: Severe haze in northern China: A synergy of anthropogenic emissions and atmospheric processes, P. Natl. Acad. Sci., 116, 8657-8666, 10.1073/pnas.1900125116, 2019.

Bond, T. C., Doherty, S. J., Fahey, D. W., Forster, P. M., Berntsen, T., DeAngelo, B. J., Flanner, M. G.,
440 Ghan, S., Kärcher, B., Koch, D., Kinne, S., Kondo, Y., Quinn, P. K., Sarofim, M. C., Schultz, M. G., Schulz, M., Venkataraman, C., Zhang, H., Zhang, S., Bellouin, N., Guttikunda, S. K., Hopke, P. K., Jacobson, M. Z., Kaiser, J. W., Klimont, Z., Lohmann, U., Schwarz, J. P., Shindell, D., Storelvmo, T., Warren, S. G., and Zender, C. S.: Bounding the role of black carbon in the climate system: A scientific assessment, J. Geophys. Res. Atmos., 118, 5380-5552, 10.1002/jgrd.50171, 2013.

445 Carlton, A. G., Bhave, P. V., Napelenok, S. L., Edney, E. O., Sarwar, G., Pinder, R. W., Pouliot, G. A., and Houyoux, M.: Model Representation of Secondary Organic Aerosol in CMAQv4.7, Environ. Sci. Technol., 44, 8553-8560, 10.1021/es100636q, 2010.

Carter, W. P. L. and Heo, G.: Development of revised SAPRC aromatics mechanisms, Atmos. Environ., 77, 404-414, 10.1016/j.atmosenv.2013.05.021, 2013.

450 Chen, L., Zhang, M., Zhu, J., and Skorokhod, A.: Model analysis of soil dust impacts on the boundary layer meteorology and air quality over East Asia in April 2015, Atmos. Res., 187, 42-56,

10.1016/j.atmosres.2016.12.008, 2017a.

Chen, Q., Fu, T.-M., Hu, J., Ying, Q., and Zhang, L.: Modelling secondary organic aerosols in China, Natl. Sci. Rev., 4, 806-809, 10.1093/nsr/nwx143, 2017b.

455 Chen, T., Liu, J., Ma, Q., Chu, B., Zhang, P., Ma, J., Liu, Y., Zhong, C., Liu, P., Wang, Y., Mu, Y., and He, H.: Measurement report: Effects of photochemical aging on the formation and evolution of summertime secondary aerosol in Beijing, Atmos. Chem. Phys., 21, 1341-1356, 10.5194/acp-21-1341-2021, 2021.

Chen, X., Wang, Z., Yu, F., Pan, X., Li, J., Ge, B., Wang, Z., Hu, M., Yang, W., and Chen, H.:
460 Estimation of atmospheric aging time of black carbon particles in the polluted atmosphere over central-eastern China using microphysical process analysis in regional chemical transport model, Atmos. Environ., 163, 44-56, 10.1016/j.atmosenv.2017.05.016, 2017c.

Cheng, Y., Zheng, G., Wei, C., Mu, Q., Zheng, B., Wang, Z., Gao, M., Zhang, Q., He, K., Carmichael, G., Pöschl, U., and Su, H.: Reactive nitrogen chemistry in aerosol water as a source of sulfate during
465 haze events in China, Sci. Adv., 2, e1601530, 10.1126/sciadv.1601530, 2016.

Chu, B., Dada, L., Liu, Y., Yao, L., Wang, Y., Du, W., Cai, J., Dällenbach, K. R., Chen, X., Simonen, P., Zhou, Y., Deng, C., Fu, Y., Yin, R., Li, H., He, X.-C., Feng, Z., Yan, C., Kangasluoma, J., Bianchi, F., Jiang, J., Kujansuu, J., Kerminen, V.-M., Petäjä, T., He, H., and Kulmala, M.: Particle growth with photochemical age from new particle formation to haze in the winter of Beijing, China, Sci.
470 Total Environ., 753, 142207, 10.1016/j.scitotenv.2020.142207, 2021.

Cirino, G. G., Souza, R. A. F., Adams, D. K., and Artaxo, P.: The effect of atmospheric aerosol particles and clouds on net ecosystem exchange in the Amazon, Atmos. Chem. Phys., 14, 6523-6543, 10.5194/acp-14-6523-2014, 2014.

Cohen, A. J., Brauer, M., Burnett, R., Anderson, H. R., Frostad, J., Estep, K., Balakrishnan, K.,
475 Brunekreef, B., Dandona, L., Dandona, R., Feigin, V., Freedman, G., Hubbell, B., Jobling, A., Kan, H., Knibbs, L., Liu, Y., Martin, R., Morawska, L., Pope, C. A., III, Shin, H., Straif, K., Shaddick, G., Thomas, M., van Dingenen, R., van Donkelaar, A., Vos, T., Murray, C. J. L., and Forouzanfar, M. H.: Estimates and 25-year trends of the global burden of disease attributable to ambient air pollution: an analysis of data from the Global Burden of Diseases Study 2015, The Lancet, 389,
480 1907-1918, 10.1016/S0140-6736(17)30505-6, 2017.

Emery, C., Tai, E., and Yarwood, G.: Enhanced Meteorological Modeling and Performance Evaluation for Two Texas Ozone Episodes, Report to the Texas Natural Resources Conservation Commission, prepared by ENVIRON, International Corp., Novato, CA, 2001.

Gu, L., Baldocchi, D., Verma, S. B., Black, T. A., Vesala, T., Falge, E. M., and Dowty, P. R.:
485 Advantages of diffuse radiation for terrestrial ecosystem productivity, J. Geophys. Res. Atmos., 107, 4050, 10.1029/2001JD001242, 2002.

Guenther, A., Karl, T., Harley, P., Wiedinmyer, C., Palmer, P. I., and Geron, C.: Estimates of global terrestrial isoprene emissions using MEGAN (Model of Emissions of Gases and Aerosols from Nature), Atmos. Chem. Phys., 6, 3181-3210, 10.5194/acp-6-3181-2006, 2006.

490 Han, Q. and Zender, C. S.: Desert dust aerosol age characterized by mass-age tracking of tracers, J. Geophys. Res. Atmos., 115, D22201, 10.1029/2010JD014155, 2010.

Held, T., Ying, Q., Kaduwela, A., and Kleeman, M.: Modeling particulate matter in the San Joaquin Valley with a source-oriented externally mixed three-dimensional photochemical grid model, Atmos.

Environ., 38, 3689-3711, 10.1016/j.atmosenv.2004.02.053, 2004.

495 Hu, J., Chen, J., Ying, Q., and Zhang, H.: One-year simulation of ozone and particulate matter in China using WRF/CMAQ modeling system, Atmos. Chem. Phys., 16, 10333-10350, 10.5194/acp-16-10333-2016, 2016.

Hu, J., Zhang, H., Ying, Q., Chen, S. H., Vandenberghe, F., and Kleeman, M. J.: Long-term particulate matter modeling for health effect studies in California – Part 1: Model performance on temporal and
500 spatial variations, Atmos. Chem. Phys., 15, 3445-3461, 10.5194/acp-15-3445-2015, 2015.

Hu, J., Zhang, H., Chen, S.-H., Wiedinmyer, C., Vandenberghe, F., Ying, Q., and Kleeman, M. J.: Predicting Primary PM2.5 and PM0.1 Trace Composition for Epidemiological Studies in California, Environ. Sci. Technol., 48, 4971-4979, 10.1021/es404809j, 2014.

Hu, J., Wang, P., Ying, Q., Zhang, H., Chen, J., Ge, X., Li, X., Jiang, J., Wang, S., Zhang, J., Zhao, Y.,
505 and Zhang, Y.: Modeling biogenic and anthropogenic secondary organic aerosol in China, Atmos. Chem. Phys., 17, 77-92, 10.5194/acp-17-77-2017, 2017.

Huang, X., Ding, A., Wang, Z., Ding, K., Gao, J., Chai, F., and Fu, C.: Amplified transboundary transport of haze by aerosol–boundary layer interaction in China, Nat. Geosci., 13, 428-434, 10.1038/s41561-020-0583-4, 2020.

510 IPCC: Climate Change 2021: The Physical Science Basis. Contribution of Working Group I to the Sixth Assessment Report of the Intergovernmental Panel on Climate Change, Cambridge University Press, Cambridge, United Kingdom and New York, NY, USA, 2021.

Irei, S., Takami, A., Sadanaga, Y., Nozoe, S., Yonemura, S., Bandow, H., and Yokouchi, Y.: Photochemical age of air pollutants, ozone, and secondary organic aerosol in transboundary air
515 observed on Fukue Island, Nagasaki, Japan, Atmos. Chem. Phys., 16, 4555-4568, 10.5194/acp-16-4555-2016, 2016.

Kleeman, M. J. and Cass, G. R.: A 3D Eulerian Source-Oriented Model for an Externally Mixed Aerosol, Environ. Sci. Technol., 35, 4834-4848, 10.1021/es010886m, 2001.

Kleeman, M. J., Robert, M. A., Riddle, S. G., Fine, P. M., Hays, M. D., Schauer, J. J., and Hannigan,
520 M. P.: Size distribution of trace organic species emitted from biomass combustion and meat charbroiling, Atmos. Environ., 42, 3059-3075, 10.1016/j.atmosenv.2007.12.044, 2008.

Lelieveld, J., Evans, J. S., Fnais, M., Giannadaki, D., and Pozzer, A.: The contribution of outdoor air pollution sources to premature mortality on a global scale, Nature, 525, 367-371, 10.1038/nature15371, 2015.

525 Li, X., Huang, L., Li, J., Shi, Z., Wang, Y., Zhang, H., Ying, Q., Yu, X., Liao, H., and Hu, J.: Source contributions to poor atmospheric visibility in China, Resources, Conservation and Recycling, 143, 167-177, 10.1016/j.resconrec.2018.12.029, 2019.

Li, Z., Guo, J., Ding, A., Liao, H., Liu, J., Sun, Y., Wang, T., Xue, H., Zhang, H., and Zhu, B.: Aerosol and boundary-layer interactions and impact on air quality, Natl. Sci. Rev., 4, 810-833,
530 10.1093/nsr/nwx117, 2017.

Liu, T., Wang, C., Wang, Y., Huang, L., Li, J., Xie, F., Zhang, J., and Hu, J.: Impacts of model resolution on predictions of air quality and associated health exposure in Nanjing, China, Chemosphere, 249, 126515, 10.1016/j.chemosphere.2020.126515, 2020.

Nenes, A., Pandis, S. N., and Pilinis, C.: ISORROPIA: A New Thermodynamic Equilibrium Model for
535 Multiphase Multicomponent Inorganic Aerosols, Aquat. Geochem., 4, 123-152,

10.1023/A:1009604003981, 1998.

Parrish, D. D., Stohl, A., Forster, C., Atlas, E. L., Blake, D. R., Goldan, P. D., Kuster, W. C., and de Gouw, J. A.: Effects of mixing on evolution of hydrocarbon ratios in the troposphere, J. Geophys. Res. Atmos., 112, D10S34, 10.1029/2006jd007583, 2007.

540 Peng, J., Hu, M., Guo, S., Du, Z., Zheng, J., Shang, D., Levy Zamora, M., Zeng, L., Shao, M., Wu, Y.-S., Zheng, J., Wang, Y., Glen, C. R., Collins, D. R., Molina, M. J., and Zhang, R.: Markedly enhanced absorption and direct radiative forcing of black carbon under polluted urban environments, P. Natl. Acad. Sci., 113, 4266-4271, 10.1073/pnas.1602310113, 2016.

Pui, D. Y. H., Chen, S.-C., and Zuo, Z.: PM2.5 in China: Measurements, sources, visibility and health
545 effects, and mitigation, Particuology, 13, 1-26, 10.1016/j.partic.2013.11.001, 2014.

Ramanathan, V., Crutzen, P. J., Kiehl, J. T., and Rosenfeld, D.: Aerosols, Climate, and the Hydrological Cycle, Science, 294, 2119-2124, doi:10.1126/science.1064034, 2001.

Robert, M. A., Kleeman, M. J., and Jakober, C. A.: Size and Composition Distributions of Particulate Matter Emissions: Part 2—Heavy-Duty Diesel Vehicles, Journal of the Air & Waste Management
550 Association, 57, 1429-1438, 10.3155/1047-3289.57.12.1429, 2007a.

Robert, M. A., VanBergen, S., Kleeman, M. J., and Jakober, C. A.: Size and Composition Distributions of Particulate Matter Emissions: Part 1—Light-Duty Gasoline Vehicles, Journal of the Air & Waste Management Association, 57, 1414-1428, 10.3155/1047-3289.57.12.1414, 2007b.

Seinfeld, J. H., Bretherton, C., Carslaw, K. S., Coe, H., DeMott, P. J., Dunlea, E. J., Feingold, G., Ghan,
555 S., Guenther, A. B., Kahn, R., Kraucunas, I., Kreidenweis, S. M., Molina, M. J., Nenes, A., Penner, J. E., Prather, K. A., Ramanathan, V., Ramaswamy, V., Rasch, P. J., Ravishankara, A. R., Rosenfeld, D., Stephens, G., and Wood, R.: Improving our fundamental understanding of the role of aerosol−cloud interactions in the climate system, P. Natl. Acad. Sci., 113, 5781-5790, doi:10.1073/pnas.1514043113, 2016.

560 Shao, P., Tian, H., Sun, Y., Liu, H., Wu, B., Liu, S., Liu, X., Wu, Y., Liang, W., Wang, Y., Gao, J., Xue, Y., Bai, X., Liu, W., Lin, S., and Hu, G.: Characterizing remarkable changes of severe haze events and chemical compositions in multi-size airborne particles (PM1, PM2.5 and PM10) from January 2013 to 2016–2017 winter in Beijing, China, Atmos. Environ., 189, 133-144, 10.1016/j.atmosenv.2018.06.038, 2018.

565 Shi, Z., Li, J., Huang, L., Wang, P., Wu, L., Ying, Q., Zhang, H., Lu, L., Liu, X., Liao, H., and Hu, J.: Source apportionment of fine particulate matter in China in 2013 using a source-oriented chemical transport model, Sci. Total Environ., 601-602, 1476-1487, 10.1016/j.scitotenv.2017.06.019, 2017.

Shu, L., Wang, T., Xie, M., Li, M., Zhao, M., Zhang, M., and Zhao, X.: Episode study of fine particle and ozone during the CAPUM-YRD over Yangtze River Delta of China: Characteristics and source
570 attribution, Atmos. Environ., 203, 87-101, 10.1016/j.atmosenv.2019.01.044, 2019.

Song, H., Lu, K., Ye, C., Dong, H., Li, S., Chen, S., Wu, Z., Zheng, M., Zeng, L., Hu, M., and Zhang, Y.: A comprehensive observation-based multiphase chemical model analysis of sulfur dioxide oxidations in both summer and winter, Atmos. Chem. Phys., 21, 13713-13727, 10.5194/acp-21-13713-2021, 2021.

575 Stohl, A., Forster, C., Eckhardt, S., Spichtinger, N., Huntrieser, H., Heland, J., Schlager, H., Wilhelm, S., Arnold, F., and Cooper, O.: A backward modeling study of intercontinental pollution transport using aircraft measurements, J. Geophys. Res. Atmos., 108, 4370, 10.1029/2002jd002862, 2003.

Sun, J., Qin, M., Xie, X., Fu, W., Qin, Y., Sheng, L., Li, L., Li, J., Sulaymon, I. D., Jiang, L., Huang, L., Yu, X., and Hu, J.: Seasonal modeling analysis of nitrate formation pathways in Yangtze River

580   Delta region, China, Atmos. Chem. Phys., 22, 12629-12646, 10.5194/acp-22-12629-2022, 2022.

Sun, Y., Jiang, Q., Wang, Z., Fu, P., Li, J., Yang, T., and Yin, Y.: Investigation of the sources and evolution processes of severe haze pollution in Beijing in January 2013, J. Geophys. Res. Atmos., 119, 4380-4398, 10.1002/2014JD021641, 2014.

Tan, T., Hu, M., Li, M., Guo, Q., Wu, Y., Fang, X., Gu, F., Wang, Y., and Wu, Z.: New insight into

585   PM2.5 pollution patterns in Beijing based on one-year measurement of chemical compositions, Sci. Total Environ., 621, 734-743, 10.1016/j.scitotenv.2017.11.208, 2018.

Wagstrom, K. M. and Pandis, S. N.: Determination of the age distribution of primary and secondary aerosol species using a chemical transport model, J. Geophys. Res. Atmos., 114, D14303, 10.1029/2009jd011784, 2009.

590   Wang, C., Wang, Y., Shi, Z., Sun, J., Gong, K., Li, J., Qin, M., Wei, J., Li, T., Kan, H., and Hu, J.: Effects of using different exposure data to estimate changes in premature mortality attributable to PM2.5 and O3 in China, Environ. Pollut., 285, 117242, 10.1016/j.envpol.2021.117242, 2021a.

Wang, G., Zhang, R., Gomez, M. E., Yang, L., Levy Zamora, M., Hu, M., Lin, Y., Peng, J., Guo, S., Meng, J., Li, J., Cheng, C., Hu, T., Ren, Y., Wang, Y., Gao, J., Cao, J., An, Z., Zhou, W., Li, G.,

595   Wang, J., Tian, P., Marrero-Ortiz, W., Secrest, J., Du, Z., Zheng, J., Shang, D., Zeng, L., Shao, M., Wang, W., Huang, Y., Wang, Y., Zhu, Y., Li, Y., Hu, J., Pan, B., Cai, L., Cheng, Y., Ji, Y., Zhang, F., Rosenfeld, D., Liss, P. S., Duce, R. A., Kolb, C. E., and Molina, M. J.: Persistent sulfate formation from London Fog to Chinese haze, P. Natl. Acad. Sci., 113, 13630-13635, 10.1073/pnas.1616540113, 2016a.

600   Wang, H. L., Qiao, L. P., Lou, S. R., Zhou, M., Ding, A. J., Huang, H. Y., Chen, J. M., Wang, Q., Tao, S. K., Chen, C. H., Li, L., and Huang, C.: Chemical composition of PM2.5 and meteorological impact among three years in urban Shanghai, China, J. Cleaner Prod., 112, 1302-1311, 10.1016/j.jclepro.2015.04.099, 2016b.

Wang, W., Liu, M., Wang, T., Song, Y., Zhou, L., Cao, J., Hu, J., Tang, G., Chen, Z., Li, Z., Xu, Z.,

605   Peng, C., Lian, C., Chen, Y., Pan, Y., Zhang, Y., Sun, Y., Li, W., Zhu, T., Tian, H., and Ge, M.: Sulfate formation is dominated by manganese-catalyzed oxidation of SO2 on aerosol surfaces during haze events, Nat. Commun., 12, 1993, 10.1038/s41467-021-22091-6, 2021b.

Wang, X., Zhang, R., Tan, Y., and Yu, W.: Dominant synoptic patterns associated with the decay process of PM2.5 pollution episodes around Beijing, Atmos. Chem. Phys., 21, 2491-2508,

610   10.5194/acp-21-2491-2021, 2021c.

Wang, X., Li, L., Gong, K., Mao, J., Hu, J., Li, J., Liu, Z., Liao, H., Qiu, W., Yu, Y., Dong, H., Guo, S., Hu, M., Zeng, L., and Zhang, Y.: Modelling air quality during the EXPLORE-YRD campaign – Part I. Model performance evaluation and impacts of meteorological inputs and grid resolutions, Atmos. Environ., 246, 118131, 10.1016/j.atmosenv.2020.118131, 2021d.

615   Wang, Y., Zhang, Q., Jiang, J., Zhou, W., Wang, B., He, K., Duan, F., Zhang, Q., Philip, S., and Xie, Y.: Enhanced sulfate formation during China's severe winter haze episode in January 2013 missing from current models, J. Geophys. Res. Atmos., 119, 10,425-410,440, 10.1002/2013JD021426, 2014.

Wang, Y., Li, W., Gao, W., Liu, Z., Tian, S., Shen, R., Ji, D., Wang, S., Wang, L., Tang, G., Song, T., Cheng, M., Wang, G., Gong, Z., Hao, J., and Zhang, Y.: Trends in particulate matter and its chemical

620 compositions in China from 2013–2017, Science China Earth Sciences, 62, 1857-1871, 10.1007/s11430-018-9373-1, 2019.

Wiedinmyer, C., Akagi, S. K., Yokelson, R. J., Emmons, L. K., Al-Saadi, J. A., Orlando, J. J., and Soja, A. J.: The Fire INventory from NCAR (FINN): a high resolution global model to estimate the emissions from open burning, Geosci. Model Dev., 4, 625-641, 10.5194/gmd-4-625-2011, 2011.

625 Wu, J. B., Wang, Z. F., Wang, Q., Li, J., Xu, J. M., Chen, H. S., Ge, B. Z., Zhou, G. Q., and Chang, L. Y.: Development of an on-line source-tagged model for sulfate, nitrate and ammonium: A modeling study for highly polluted periods in Shanghai, China, Environ. Pollut., 221, 168-179, 10.1016/j.envpol.2016.11.061, 2017.

Xie, X., Ying, Q., Zhang, H., and Hu, J.: Spatial and Temporal Variations in the Atmospheric Age
630 Distribution of Primary and Secondary Inorganic Aerosols in China, Engineering, 10.1016/j.eng.2022.03.013, 2022a.

Xie, X., Shi, Z., Ying, Q., Zhang, H., and Hu, J.: Age-Resolved Source and Region Contributions to Fine Particulate Matter During an Extreme Haze Episode in China, Geophys. Res. Lett., 48, e2021GL095388, 10.1029/2021GL095388, 2021.

635 Xie, X., Wang, T., Yue, X., Li, S., Zhuang, B., and Wang, M.: Effects of atmospheric aerosols on terrestrial carbon fluxes and CO_2 concentrations in China, Atmos. Res., 237, 104859, 10.1016/j.atmosres.2020.104859, 2020.

Xie, X., Hu, J., Qin, M., Guo, S., Hu, M., Wang, H., Lou, S., Li, J., Sun, J., Li, X., Sheng, L., Zhu, J., Chen, G., Yin, J., Fu, W., Huang, C., and Zhang, Y.: Modeling particulate nitrate in China: Current
640 findings and future directions, Environ. Int., 166, 107369, 10.1016/j.envint.2022.107369, 2022b.

Xu, W., Sun, Y., Wang, Q., Zhao, J., Wang, J., Ge, X., Xie, C., Zhou, W., Du, W., Li, J., Fu, P., Wang, Z., Worsnop, D. R., and Coe, H.: Changes in Aerosol Chemistry From 2014 to 2016 in Winter in Beijing: Insights From High-Resolution Aerosol Mass Spectrometry, J. Geophys. Res. Atmos., 124, 1132-1147, 10.1029/2018JD029245, 2019.

645 Yang, Y. R., Liu, X. G., Qu, Y., An, J. L., Jiang, R., Zhang, Y. H., Sun, Y. L., Wu, Z. J., Zhang, F., Xu, W. Q., and Ma, Q. X.: Characteristics and formation mechanism of continuous hazes in China: a case study during the autumn of 2014 in the North China Plain, Atmos. Chem. Phys., 15, 8165-8178, 10.5194/acp-15-8165-2015, 2015.

Ying, Q. and Kleeman, M. J.: Source contributions to the regional distribution of secondary particulate
650 matter in California, Atmos. Environ., 40, 736-752, 10.1016/j.atmosenv.2005.10.007, 2006.

Ying, Q., Fraser, M. P., Griffin, R. J., Chen, J., and Kleeman, M. J.: Verification of a source-oriented externally mixed air quality model during a severe photochemical smog episode, Atmos. Environ., 41, 1521-1538, 10.1016/j.atmosenv.2006.10.004, 2007.

Ying, Q., Zhang, J., Zhang, H., Hu, J., and Kleeman, M. J.: Atmospheric Age Distribution of Primary
655 and Secondary Inorganic Aerosols in a Polluted Atmosphere, Environ. Sci. Technol., 55, 5668-5676, 10.1021/acs.est.0c07334, 2021.

Zhang, H., Guo, H., Hu, J., Ying, Q., and Kleeman, M. J.: Modeling Atmospheric Age Distribution of Elemental Carbon Using a Regional Age-Resolved Particle Representation Framework, Environ. Sci. Technol., 53, 270-278, 10.1021/acs.est.8b05895, 2019a.

660 Zhang, J., Yuan, Q., Liu, L., Wang, Y., Zhang, Y., Xu, L., Pang, Y., Zhu, Y., Niu, H., Shao, L., Yang, S., Liu, H., Pan, X., Shi, Z., Hu, M., Fu, P., and Li, W.: Trans-Regional Transport of Haze Particles

From the North China Plain to Yangtze River Delta During Winter, J. Geophys. Res. Atmos., 126, e2020JD033778, 10.1029/2020JD033778, 2021.

Zhang, Q., Zheng, Y., Tong, D., Shao, M., Wang, S., Zhang, Y., Xu, X., Wang, J., He, H., Liu, W., Ding, Y., Lei, Y., Li, J., Wang, Z., Zhang, X., Wang, Y., Cheng, J., Liu, Y., Shi, Q., Yan, L., Geng, G., Hong, C., Li, M., Liu, F., Zheng, B., Cao, J., Ding, A., Gao, J., Fu, Q., Huo, J., Liu, B., Liu, Z., Yang, F., He, K., and Hao, J.: Drivers of improved $PM_{2.5}$ air quality in China from 2013 to 2017, P. Natl. Acad. Sci., 116, 24463-24469, 10.1073/pnas.1907956116, 2019b.

Zheng, B., Zhang, Q., Zhang, Y., He, K. B., Wang, K., Zheng, G. J., Duan, F. K., Ma, Y. L., and Kimoto, T.: Heterogeneous chemistry: a mechanism missing in current models to explain secondary inorganic aerosol formation during the January 2013 haze episode in North China, Atmos. Chem. Phys., 15, 2031-2049, 10.5194/acp-15-2031-2015, 2015a.

Zheng, B., Tong, D., Li, M., Liu, F., Hong, C., Geng, G., Li, H., Li, X., Peng, L., Qi, J., Yan, L., Zhang, Y., Zhao, H., Zheng, Y., He, K., and Zhang, Q.: Trends in China's anthropogenic emissions since 2010 as the consequence of clean air actions, Atmos. Chem. Phys., 18, 14095-14111, 10.5194/acp-18-14095-2018, 2018.

Zheng, G. J., Duan, F. K., Su, H., Ma, Y. L., Cheng, Y., Zheng, B., Zhang, Q., Huang, T., Kimoto, T., Chang, D., Pöschl, U., Cheng, Y. F., and He, K. B.: Exploring the severe winter haze in Beijing: the impact of synoptic weather, regional transport and heterogeneous reactions, Atmos. Chem. Phys., 15, 2969-2983, 10.5194/acp-15-2969-2015, 2015b.

Figures
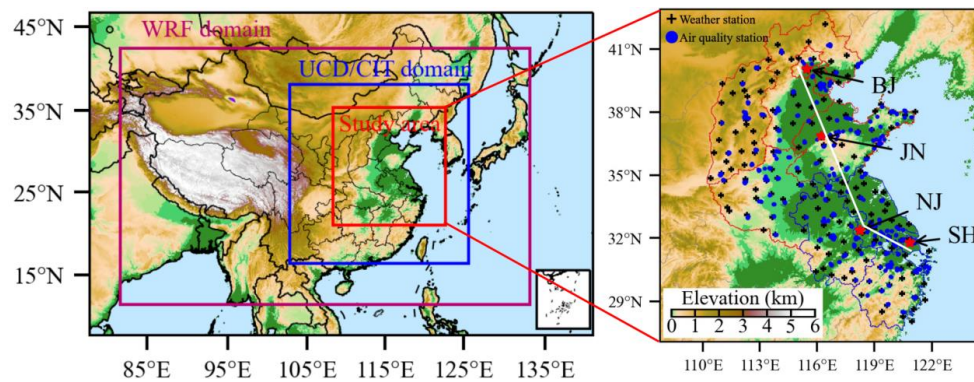
Figure 1. Modeling domains and the locations of the observation stations. Black crosses represent the
weather stations and the blue dots represent the air quality stations. Four main cities (BJ: Beijing, JN:
Jinan, NJ: Nanjing, SH: Shanghai) in eastern China are also marked by red stars.

685
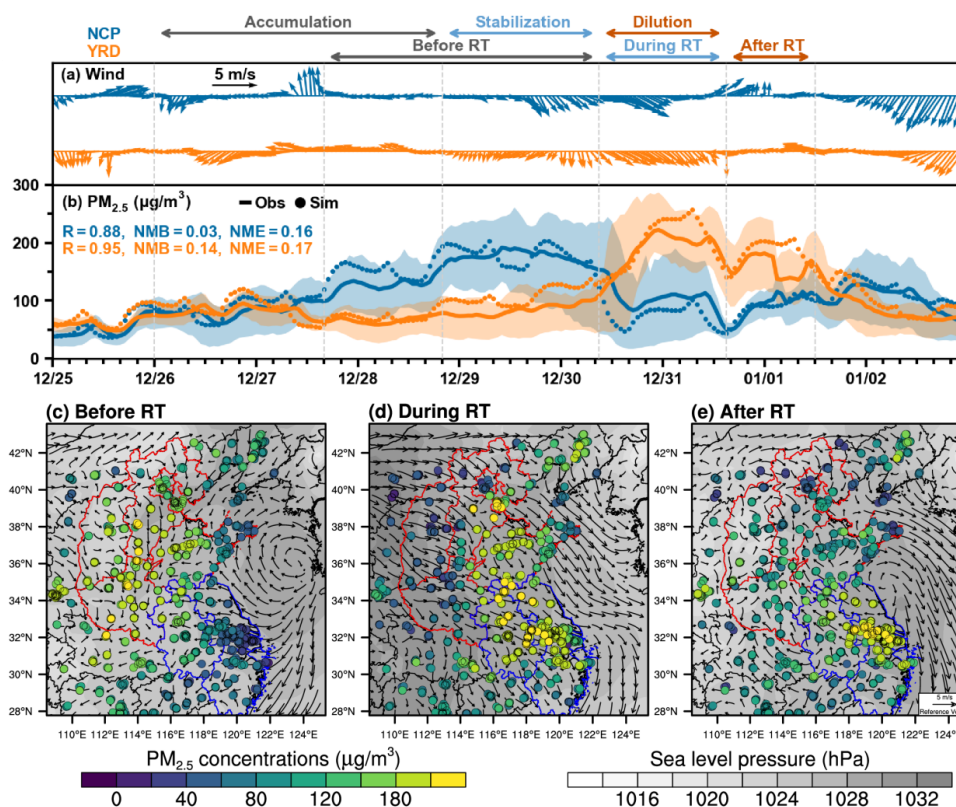
Figure 2. Time series and spatial distributions of wind fields and PM$_{2.5}$ during this haze episode. **(a, b)** Observed wind and PM$_{2.5}$ concentrations in NCP and YRD. Shaded areas represent the 25th–75th percentile range of observation. Solid dots mark the simulated PM$_{2.5}$ concentrations. **(c–e)** Observed PM$_{2.5}$ concentrations, WRF-simulated wind fields, and sea level pressure before, during, and after regional transport (RT).
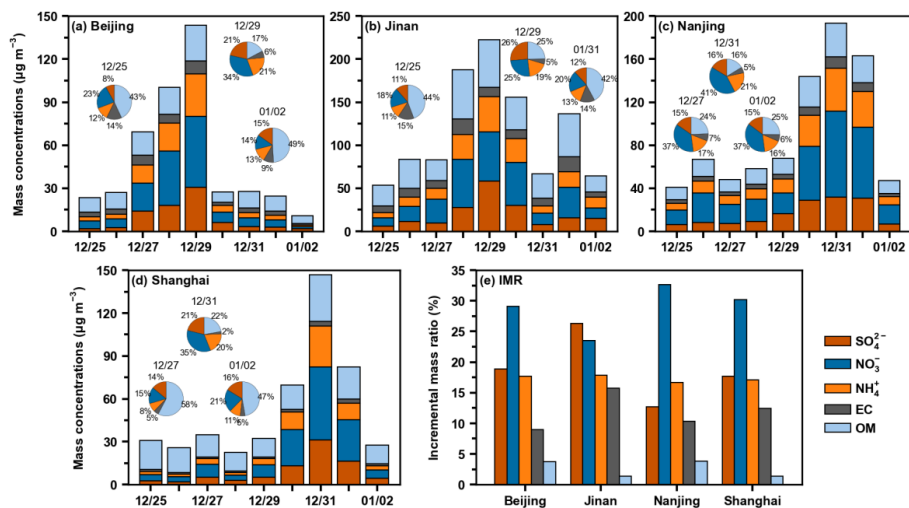
Figure 3. Mass concentrations and fractions **(a–d)** and incremental mass ratio (e) of the major $PM_{2.5}$ chemical compositions (SO_4^{2-}, NO_3^-, NH_4^+, EC, and OM) in Beijing, Jinan, Nanjing, and Shanghai.
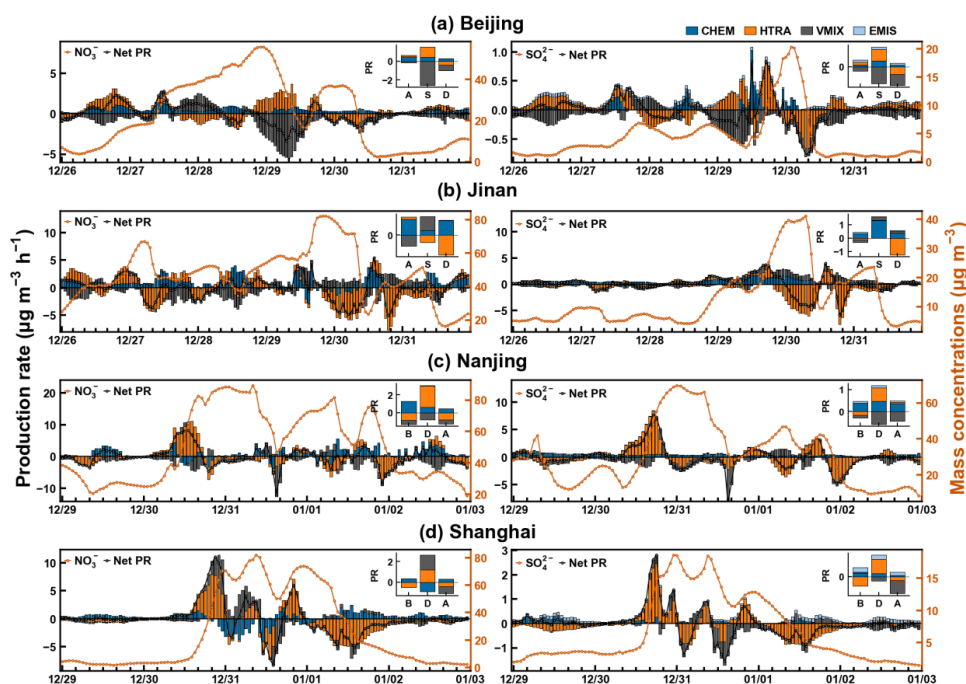
Figure 4. The contributions of physical/chemical processes (CHEM: gas-phase, aerosol, and cloud chemistry; VMIX: vertical mixing and dry deposition; HTRA: horizontal advection; EMIS: emission) to NO_3^- and SO_4^{2-} concentrations within the first 10 layers in Beijing, Jinan, Nanjing, and Shanghai. The stacked bar graphs inserted in each panel represent the total contribution during the corresponding period. A, S, and D indicate the accumulation, stabilization, and dilution stage in Beijing and Jinan; and B, D, and A represent the period before, during, and after regional transport in Nanjing and Shanghai.
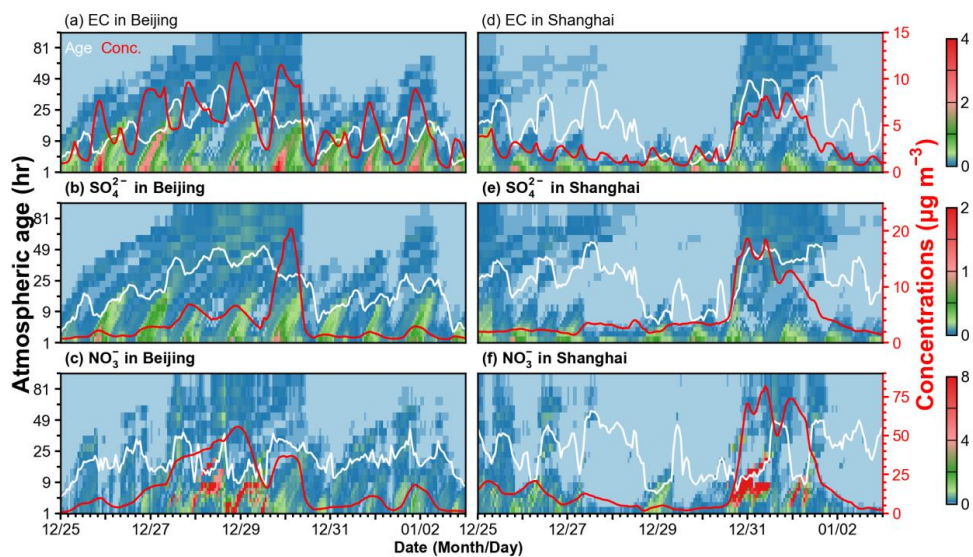
Figure 5. Hourly atmospheric age distribution of EC, SO_4^{2-}, and NO_3^- in Beijing and Shanghai during this haze episode. White lines represent the average atmospheric age, and red lines (right y-axis) indicate total mass concentrations. The results were combined from simulations with age-bin updating intervals of 1, 3, 6, 8, and 12 h.
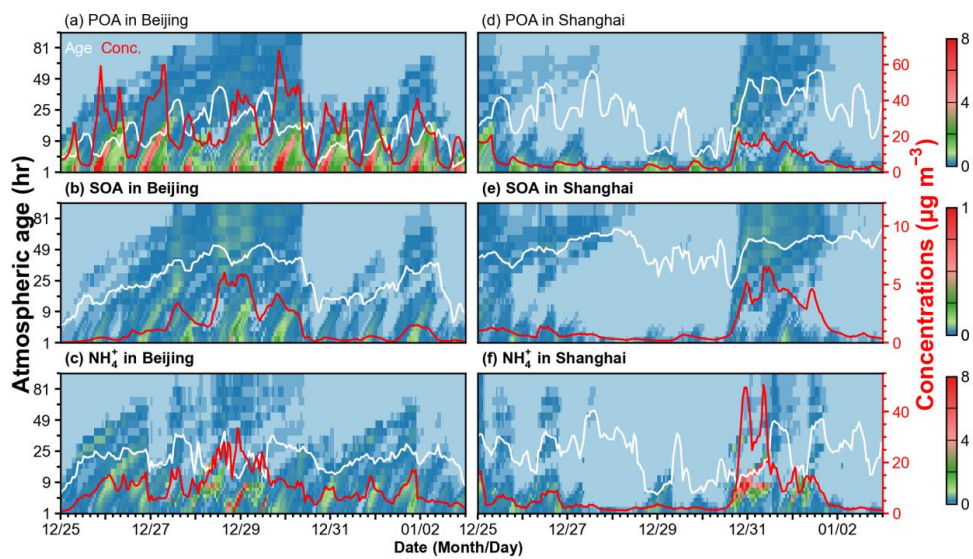
715

**Figure 6.** Same as **Figure 5** but for POA, SOA, and NH₄⁺.
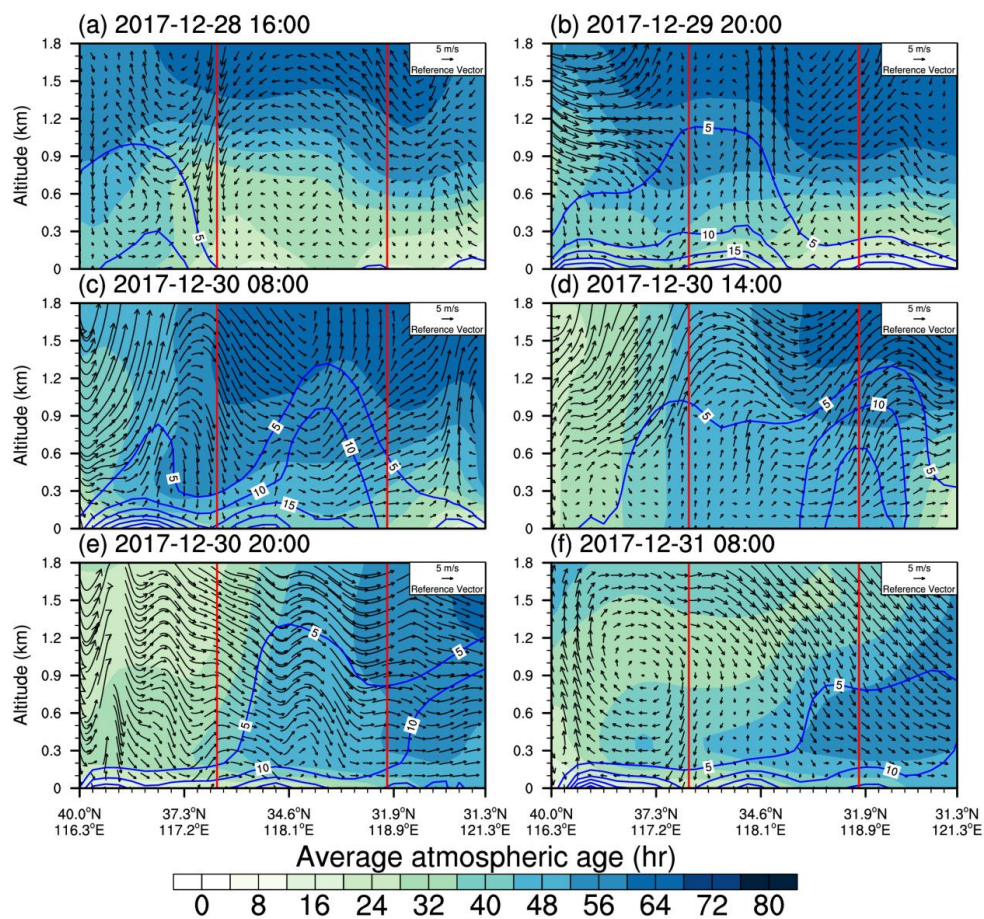
Figure 7. Vertical cross section of the average atmospheric age (color contours; h) and concentrations
(blue solid lines; µg m⁻³) of EC along the transport route from Beijing to Shanghai (white solid line
in **Figure 1**) at **(a)** 16:00 LT 28 December, **(b)** 20:00 LT 29 December, **(c–e)** 08:00, 14:00, 20:00 LT
30 December, and **(f)** 08:00 LT 31 December 2017. Note that the vertical wind speed was multiplied
by 500 for the illustration of vertical circulations. The location of Jinan and Nanjing are marked as red
solid lines.
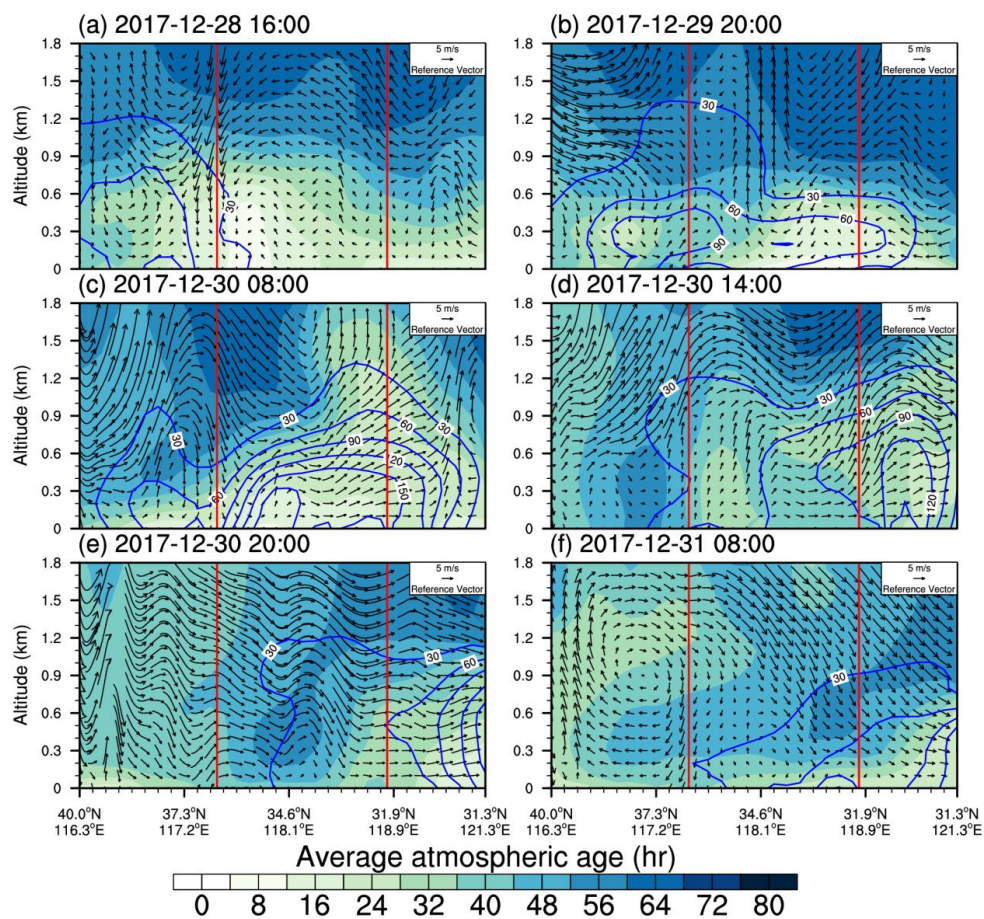
Figure 8. Same as **Figure 7** but for NO_3^-.
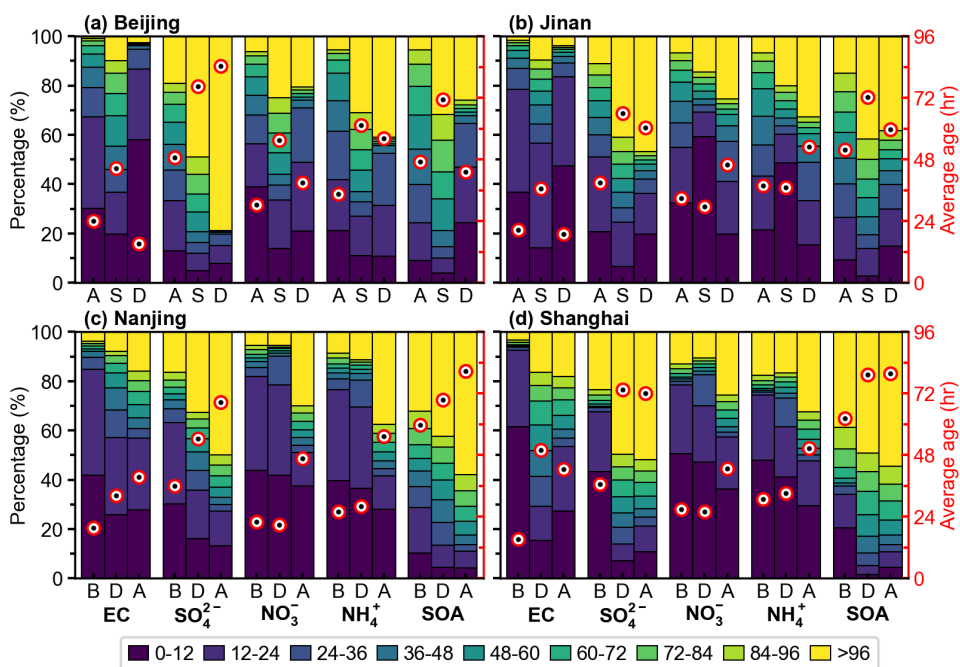
Figure 9. The mass fractional contributions of different age bins to EC, SO_4^{2-}, NO_3^-, NH_4^+, and SOA in Beijing, Jinan, Nanjing, and Shanghai. The red circle with a black dot indicates the average atmospheric age (in hours, right y-axis). A, S, and D indicate the accumulation, stabilization, and dilution stage in Beijing and Jinan; B, D, and A represent the period before, during, and after regional transport in Nanjing and Shanghai.
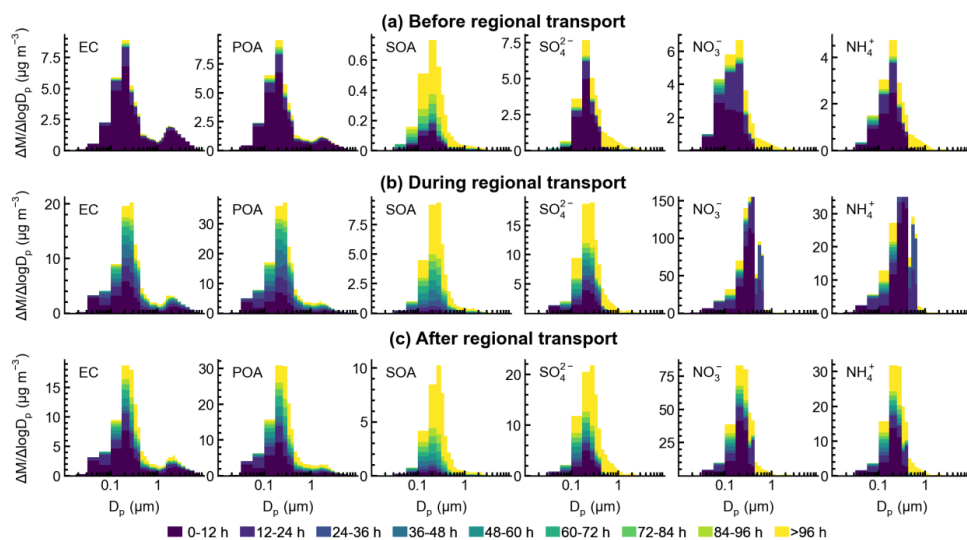
735

Figure 10. The size distribution of EC, POA, SOA, SO_4^{2-}, NO_3^-, and NH_4^+ in Shanghai (a) before, (b) during, and (c) after regional transport.